Title	Effect of fast pyrolysis conditions on biomass solid residues at high temperatures
Author(s)	Trubetskaya, Anna; Jensen, Peter Arendt; Jensen, Anker Degn; Garcia Llamas, Angel David; Umeki, Kentaro; Glarborg, Peter
Publication Date	2015-12-03
Publication Information	Trubetskaya, A., Jensen, P. A., Jensen, A. D., Garcia Llamas, A. D., Umeki, K., & Glarborg, P. (2016). Effect of fast pyrolysis conditions on biomass solid residues at high temperatures. Fuel Processing Technology, 143, 118-129. doi: https://doi.org/10.1016/j.fuproc.2015.11.002
Publisher	Elsevier
Link to publisher's version	https://doi.org/10.1016/j.fuproc.2015.11.002
Item record	http://hdl.handle.net/10379/7355
DOI	http://dx.doi.org/10.1016/j.fuproc.2015.11.002

Effect of fast pyrolysis conditions on biomass solid residues at high temperatures

Anna Trubetskaya[a,**], Peter Arendt Jensen[a], Anker Degn Jensen[a], Angel David Garcia Llamas[b], Kentaro Umeki[b], Peter Glarborg[a,*]

[a]*Department of Chemical and Biochemical Engineering, Technical University of Denmark, Søltofts Plads Bygning 229, Kgs. Lyngby 2800, Denmark*
[b]*Department of Engineering Sciences and Mathematics, Devision Energy Science, Luleå University of Technology, 97187, Luleå, Sweden*

Abstract

Fast pyrolysis of wood and straw was conducted in a drop tube furnace (DTF) and compared with corresponding data from a wire mesh reactor (WMR) to study the influence of temperature (1000-1400)°C, biomass origin (pinewood, beechwood, wheat straw, alfalfa straw), and heating rate (10^3°C/s, 10^4°C/s) on the char yield and morphology. Scanning electron microscopy (SEM), elemental analysis, and ash compositional analysis were applied to characterize the effect of operational conditions on the solid residues (char, soot) and gaseous products. The char yield from fast pyrolysis in the DTF setup was 3 to 7 % (daf) points lower than in the WMR. During fast pyrolysis pinewood underwent drastic morphological transformations, whereas beechwood and straw samples retained the original porous structure of the parental fuel with slight melting on the surface. The particle size of Danish wheat straw char decreased in its half-width with respect to the parental fuel, whereas

*Corresponding author. pgl@kt.dtu.dk
**Corresponding author. atru@kt.dtu.dk

the alfalfa straw char particle size remained unaltered at higher temperatures. Soot particles in a range from 60 to 300 nm were obtained during fast pyrolysis. The soot yield from herbaceous fuels was lower than from wood samples, possibly due to differences in the content of lignin and resin acids.
Keywords: fast pyrolysis, drop tube furnace, wire mesh reactor, soot, CAMSIZER XT

1. Introduction

Suspension firing of biomass is widely used for power generation and has been considered as an important step in reduction of greenhouse gas emissions. Unlike coal, biomass is difficult to mill to $< 100\,\mu$m due to its fibrous structure, resulting in higher energy consumption for the comminution process. The shape and size distribution of ground biomass particles consists of a larger fraction of flake- and cylinder-like particles with a particle size $> 300\,\mu$m. In biomass suspension firing, it is a challenge to achieve high fuel conversion at the short residence time while minimizing the input for milling. This is further challenged by application of a broad biofuel range to obtain high operational flexibility at power plants. Thus an increased energy input into the biomass comminution process affects the total efficiency of a power plant, and large particle sizes may cause problems with flame stability and burnout.

In suspension firing, biomass particles are heated rapidly to high temperatures of 1000-1400°C, leading to volatile release and formation of solid residues (char and soot) during devolatilization. The solid residue yield and its properties, including particle size and shape, composition, reactivity and

burnout, depend strongly on the operational conditions of fast devolatilization [1–4]. A number of studies [5–11] have investigated structural changes of different biomass types and their plant cell components during fast pyrolysis. Sharma et al. [5–7, 12] reported structural changes of lignin and tobacco char at temperatures up to 750°C with rapid heating rates, accompanied by softening and melting of a solid phase. The effect of char plasticization was observed mostly at high heating rate of pyrolysis ($> 10^3$°C/s) [8, 9, 13–15]. The char fluidity of coal and lignin during pyrolysis was described by the FG-DVC model (Functional Group - Depolymerization, Vaporization and Cross-linking model) of Solomon et al. [16, 17]. They pointed out that the char fluidity is influenced by small differences in the cross-linking rate with oxygen, affecting cross-linking and preventing char fluidity [18].

Previous investigations of biomass pyrolysis [9, 15, 19, 20] ascribed the char structural transformations and changes in reactivity to the catalytic effect of minerals (K, Ca, Mg and Si). Wornat et al. [19] reported migration of alkali and alkaline earth metals to the particle surface for high oxygen content fuels, with the formation of beads on the char shell, accompanied by a highly cross-linked carbon structure that hindered crystallite mobility and graphitization during combustion. Dall'Ora et al. [9] studied fast pyrolysis of beechwood in an entrained-flow reactor, and concluded that calcium and potassium catalyze cross-linking, resulting in a higher char yield and less severe char morphological changes.

In the present study the relation between different types of biomass and their solid residue (char, soot) properties was investigated. Char and soot yields were obtained from fast pyrolysis in a drop tube furnace (DTF). The

char yields from the DTF were compared with results from a wire mesh reactor (WMR) [21] at temperatures $> 1000°C$ to study the simultaneous effect of temperature, heating rate, and biomass origin on the char yield. The influence of extractives on the structural changes, on which available literature is not extensive, was also studied using char from the DTF. This work also attempted to fill a gap about the effect of biomass origin on the soot formation during fast pyrolysis. The influence of ash composition, particularly of K and Ca elements, on the char morphological changes under fast heating was characterized by SEM and TEM microscopy.

2. Materials and methods

2.1. Original biomass characterization

Pinewood, beechwood, Danish wheat straw, and alfalfa straw were selected for the fast pyrolysis study in the DTF and WMR. The wheat straw was leached in deionized water (room temperature) by continuous stirring for 12 hours, followed by drying at 30°C in an oven desiccator without any ventilation. The mineral content after biomass leaching was determined by ash analysis. Due to the wheat straw leaching, the metal content was reduced to $\approx 60\,\%$ of the original value and the Cl, S, K, Na and P contents were strongly reduced [21]. The leached wheat straw was selected to study the influence of alkali on the char and soot yields.

The proximate and ultimate analyses of fuels are shown in Table 1. The fuels were milled on a Retsch rotor mill RZ200 and sieved to a particle size fraction of 0.2-0.425 mm. The wood and herbaceous fuels were selected for the present study, based on the differences in organic and inorganic matter.

The compositional analysis of biomass (cellulose, hemicellulose, acid-soluble lignin, acid-insoluble lignin, protein and extractives) was conducted according to NREL technical reports [22–24] and Thammasouk et al. [25], and shown in Table 2.

The water-ethanol extraction was performed on wheat straw and alfalfa straw which contain a high level of hydrophilic and lipophilic extractable compounds as described by Thammasouk et al. [25]. Extraction with acetone on pinewood and beechwood was done for the quantitative estimation of extractives in the original biomass, and to remove resin and fatty acids, waxes, and phytosterols for the investigation of char structural changes under fast heating as described in the supplemental material.

2.2. Experimental apparatus and procedure

2.2.1. Drop Tube Furnace

The Drop Tube Furnace (DTF) used in the present study is shown in Figure 1. The cylindrical reactor tube was made of alumina ceramic (grade C799) with an inner diameter of 54 mm. The reactor tube was heated by tube furnace modules using SiC rods as heating elements (Elite Thermal Systems Ltd.) with a maximum temperature of 1500°C. Supply of primary gas was led through the biomass feeder, and secondary gas was led to the top of the reactor through a packed bed of ceramic balls that distributed the gas flow equally in the radial direction. Inlet gas flows of O_2, N_2, H_2, CO and CO_2 were controlled by mass flow controllers (EL-FLOW® Select, Bronkhorst High-Tech B.V.), while the flow rate of H_2O was controlled by a syringe pump (Legato 100, KD Scientific Inc.). A syringe pump type biomass feeder

was used to supply biomass at low feeding rates [26]. The feeding probe was water-cooled at 20°C to ensure a high heating rate of the biomass when it entered the reactor. The Reynolds number of the gas flow inside the reactor was 60-100, dependent on the reaction temperature.

Biomass was rapidly heated and reacted while it fell down through the reactor. Reaction products were separated into coarse particles (mainly char and fly ashes), fine particles (mainly soot and precipitated ash vapor), and permanent gases. Soot particles passing the cyclone (cut size 2.5 μm) were captured from the product gas flow by a grade QM-A quartz filter with a diameter of 50 mm (Whatman, GE Healthcare Life Science). The larger particles (e.g. char) could either fall down to a char bin or a stainless steel cyclone with cut size of 2.5 μm (URG-2000-30ENS-1, URG Corporation). After an activated carbon filter (VACU-GUARD 150, GE Healthcare Life Science), the gas composition was measured by a micro gas chromatograph (Model 490, Agilent Technologies). The μGC was equipped with two columns (CP-MolSieve 5 A for H_2, O_2, N_2, CH_4 and CO; and PoraPlot U for CO_2, C_2H_4, C_2H_6, C_2H_2, and C_3H_6/C_3H_8) and thermal conductivity detectors. The temperature of the char bin and product gas was controlled by heating controllers (HTC-5500, Hemi Heating AB) with thermo-tapes (S-type, Hemi Heating AB) and kept at 200°C to avoid tar condensation.

In the present study, the experiments were conducted by feeding ≈ 5 g of biomass at a rate of 0.2 g/min. Both primary and secondary gases were N_2, and the flow rate of primary gas was 180 mL /min and that of secondary gas was 4.8 L /min. The residence time of the fuel particles was estimated to be about 1 s, taking into account the density change during pyrolysis [11].

Three reaction temperatures (1000, 1250 and 1400°C) were applied.

2.2.2. Wire mesh reactor

The wire mesh reactor at TU Munich used in this study was previously described by Tremel et al. [27]. A schematic drawing is shown in the supplemental material (Figure S-2). It could be operated up to a temperature of 1700°C, at a heating rate of 5000°C/s, and a maximal pressure of 50 bar.

2.2.3. Measurement uncertainty

For the DTF, the measurement error was calculated for each component of a mass balance (C_xH_y+vapor, gas, coke, soot). The absolute extended uncertainty of the product yield was determined by a Gaussian error propagation procedure [28], based on the equations shown in the supplemental material (S-4). The average standard measurement error in the present study was ±2 wt. %, within a 95 % confidence interval for the DTF experiments. The volatile measurements with a micro gas chromatograph and soot loss in the DTF setup were sources of experimental error (< 15 %) as shown in the calculated carbon / hydrogen balances. Another source of error was the non-measured fractions of vapor, tars and larger hydrocarbons in the DTF.

For the WMR, the error bars represent the standard deviation from the mean of the series of experiments at each condition [21]. The char yield data obtained in the wire mesh reactor were plotted as a representative average of at least five experiments. The measurement uncertainties of the char yields, prepared in the WMR, were < 6%. The inaccuracy in determining the char yield was mainly caused by weighting errors.

2.2.4. Solid residue characterization

Three different solid residues were distinguished in the present study, namely char, soot and coke. Char and soot were collected in a char bin and on a filter at the different experimental temperatures. Char is the fraction of non-devolatilized solid from the initial biomass, consisting mainly of carbon and ash with minor presence of hydrogen and oxygen. Coke, the carbonaceous material deposited on the reactor walls, was quantified after each experiment by measurement of the concentration of CO_2 during oxidation.

SEM and TEM microscopy. SEM analysis of char was performed on a microscope (FEI Company, Inspect) with a tungsten filament under high vacuum in order to understand char structural and chemical properties. Prior to the analysis, char samples were coated with a thin layer of carbon (40 sec, 5 mA) using a Cressington 208 Carbon Coater to avoid sample charging.

Soot samples were studied on the transmission electron microscope (200-kV FEI Tecnai T20 G^2). Prior to the microscopy, soot samples were kept at 350°C for 4 hours in a thermo-gravimetric instrument (TGA) to reduce the amount of volatiles. The TGA curves shown in the supplemental material (Figure S-7) quantified the remaining volatiles yield to be $< 5\%$. TEM analysis of soot was performed using dry method to avoid nano-structure changes as shown in the supplemental material (Figure S-8). In addition, soot samples were grounded a very short time using a pestle and mortar, to ensure homogeneous particle distribution, and placed on a Cu grid. Imaging of soot samples was performed in vacuum using a Gatan 894 2K UltraScan 1000 CCD camera and a FEI single-tilt holder.

Elemental analysis. The elemental analysis was performed on two instruments of the same model (Eurovector, model EA3000). Acetanilide was used as a reference standard. The ash content was determined using a standard ash test at 550°C, according to the procedure described in DIN EN 14775.

Ash compositional analysis. The ash compositional analysis was performed by an X-ray fluorescence instrument (Shimadzu, model EDX 800-HS) at TU Munich. Prior to the XRF analysis, char samples were pre-heated in oxygen at 5°C/min up to 550°C and kept at that temperature for 7 h. The generated ash (about 200 mg) was initially mixed and then pressed with a special wax (mixture ratio 1:5). The Cl and S content in the ash was analyzed by ICP-OES/IC at TU Wien. The ash sample was dissolved in ultrapure water at 120°C for 1 h, and then the solution was filtered and analyzed by ICP-OES/IC.

Particle size and shape. The particle size and shape of the original biomass and its char were characterized on a 2D dynamic imaging instrument (CAMSIZER XT, Retsch), designed for a particle size range of 3 μm to 3 mm. A particle shadow was captured by the CCD-basic and zoom cameras of the CAMSIZER XT. The zoom-camera was optimized to analyze smaller particles with a high resolution, whereas the basic-camera detected larger particles due to a large field of view. The projected area of a particle was analyzed by the CAMSIZER XT 6.3.10 software to characterize its size and shape. Fine biomass particles tended to agglomerate which made it difficult to detect the true geometric dimensions of each individual particle. Therefore, the particle agglomerates were separated without destroying the primary particles

by air pressure dispersion. For the particle size analysis, ca. 100 mg of sample was used. The particle size and shape measurements of char, collected from several drop tube pyrolysis experiments, were performed twice with the CAMSIZER XT for each operational condition to establish reproducible results.

The Martin minimal ($x_{Ma,min}$) and Feret maximal ($x_{Fe,max}$) diameters are suitable parameters to represent the biomass particle width and length in combustion. The Martin diameter is a chord length that divides the projected particle area into two equal halves [29], as shown in the supplemental material (Figure S-5). The minimal Martin diameter ($x_{Ma,min}$) is determined from the smallest Martin diameter of the particle projection [30], and represents a particle width based on the assumption of a biomass particle to be thinner than its width in the diffusion process in combustion. The Feret diameter is the distance between two tangents placed perpendicular to the measurement direction [29], as shown in the supplemental material (Figure S-5). The Feret maximal diameter is applied as the largest value of all measured Feret diameters of a particle [30], and the longest measurable diameter $x_{Fe,max}$ is the largest diameter to fulfill the assumption that the length of a particle has to be larger than its width. The results of the particle size analysis were represented as a frequency distribution over $x_{Ma,min}$, as defined in equation 1:

$$q_3(x_{Ma,min}) = \frac{dQ_3(x_{Ma,min})}{x(x_{Ma,min})} \tag{1}$$

where Q_3 is the cumulative particle size distribution based on volume. The particle shape was characterized by sphericity (SPHT) and aspect ratio (b/l) in the present study. Sphericity is one of the most common ways to express

the deviation of an 2D image shape from a sphere and is defined by equation 2:

$$SPHT = \frac{4 * \pi * A}{P^2} \tag{2}$$

where P is the measured circumference of a particle projection and A is the measured area of a particle projection. The particle is considered to be spherical when the value of sphericity is equal to one and non-spherical when it is smaller than one. The aspect ratio (AR) is defined as the ratio of particle width (b = $x_{Ma,min}$) to the particle length (l = $x_{Fe,max}$).

$$AR = \frac{b}{l} \tag{3}$$

3. Results and discussion

3.1. Carbon and hydrogen balances

The mass balances of the DTF experiments with respect to measured solid residues (char, soot, coke) and major gaseous products (CO_2, H_2, CO, CH_4, C_3H_8, C_2H_4, C_2H_2) in dependency on the heat treatment temperature are shown in Figure 2. The amount of vapor, tars, and larger hydrocarbons was not measured in the present study, but estimated by difference from the mass balance. The carbon and hydrogen balances represent an average of at least two measurements. During fast pyrolysis, mainly gaseous products were formed, along with lower amounts of solid residues at higher temperatures.

At 1000°C, the yield of larger hydrocarbons and vapor was significantly larger than at higher temperatures. The carbon in wood and herbaceous biomasses was converted to gas, soot and char. Hydrogen was present mostly in gaseous products, tars, larger hydrocarbons and vapor at 1000°C. Almost

all hydrogen (> 90 %) was found in the form of gaseous products above 1250°C for wood and herbaceous biomasses. Higher temperatures suppressed tar formation and enhanced hydrogen and oxygen release to gaseous products.

3.2. The solid product yield

Char yield. The wire mesh reactor (WMR) results were obtained by Trubetskaya et al. [21]. In that study, the char yield (daf) was represented including inorganic matter in char relative to the biomass on dry and ash-free basis. In the present work, char yields of wood and herbaceous biomass in both reactors are shown on dry ash free basis (daf), excluding inorganic matter in char relative to original biomass (daf) in Figure 3. The biomass char yield at fast pyrolysis conditions depends strongly on the biomass origin, temperature and heating rate. Straw (herbaceous) samples showed higher char yields compared with wood and leached wheat straw due to the presence of alkali metals as known from the literature [15, 19, 20, 31]. The char yields of pinewood and beechwood showed significant differences, possibly due to differences in lignin content, presence of temperature stable extractives, and alkali metal content (higher in beechwood).

As a general trend, the char yield of beechwood, wheat straw and alfalfa straw decreased with increasing temperature, indicating a dependency of the char yield on the heat treatment temperature. On the other hand, the char yield of pinewood and leached wheat straw decreased only slightly between 1000 and 1400°C, being lower than the char yield of other fuels at 1000°C. The continuous decrease in char yield from wheat straw (rich in K, Si) and alfalfa straw (rich in Ca, K) was attributed partly to high-temperature ash

reactions, leading to the volatile ash release, and affecting the organic matter release. The results indicate that the influence of alkali on the char yield is more pronounced at low and intermediate heating rates than at fast heating rates in the DTF as shown in Figure S-11.

The results showed that there is a clear difference between char yields in the WMR and DTF. The char yield in the DTF was 3-7 % wt. (daf) lower than that in the WMR, possibly due to the differences in heating rate and residence time. The pyrolysis in the WMR was carried out with a lower heating rate (1000°C/s) than in the DTF (10^4-10^5°C/s). When the holding time in the WMR was increased from 1 to 2 s, the char yield became slightly lower [21].

Soot yield. Figure 4 shows the soot and char yields, each separated into organic matter and ash. The soot yield varied between different biomasses at similar operational conditions. The highest soot yield was observed during pinewood fast pyrolysis. The soot yield increased with temperature, reaching a peak value at 1250°C, and slightly decreased at higher temperatures, corresponding to the well-known soot yield curvature [32].

Figure 4 shows large differences in the soot yield of wood, leached wheat straw and herbaceous biomass. The fact that beechwood and leached wheat straw exhibit major differences in soot yield despite similar alkali (i.e. K^+) and holocellulose contents indicate that these parameters are of minor importance for the soot fraction. Instead, lignin and extractives in the original biomass possibly are important for the soot yield. The leaching of alkali from wheat straw resulted in a removal of lignin and other organic compounds as shown in Table 2, leading to the decreased formation of PAH precursors, and

thereby to lower soot yields. Williams et al. [33] suggested that biomass with a high content of lignin may form larger soot fractions due to its ability to generate phenolic tars. A significant fraction of aromatic tars and soot originates from lignin pyrolysis, mainly composed of guaiacol and syringol-type units [34–36]. Ross et al. [37] stated that wood soot contains PAH material, promoted by the presence of acetylene at higher temperatures. The suggestion is consistent with the gas measurement results of the present study. The measured C_2H_2 concentration is up to 0.05 vol. % in inert nitrogen during fast pyrolysis of wood and herbaceous biomasses at 1000°C shown in Figure 5. With increasing temperature, the C_2H_2 yield decreased, whereas the soot yield increased. Moreover, C_2H_4 might affect the soot yield at high temperatures, facilitating PAH molecule growth [37]. The high concentration of resin acids in pinewood could increase the soot yield in addition to a stronger formation of PAH precursors [38, 39].

3.3. Volatile gas composition

The concentrations of H_2, CO, CO_2 and C_xH_y (CH_4, C_2H_2, C_2H_4) are shown in Figure 5. The gas composition changed significantly with increasing heat treatment temperature. Higher temperatures favor cracking of the volatile hydrocarbon products, increasing the yield of H_2 generated mainly from dehydrogenation. Soot formation could lead to increase in the yields of H_2 and CO between 1000 and 1250°C due to polymerization and dry

reforming reactions, equations 4 and 5.

$$\text{Hydrocarbon polymerization}: \ C_nH_m \rightarrow \left(\frac{m}{2}\right) H_2 + nC_{soot} \tag{4}$$

$$\text{Dry reforming}: \ C_nH_m + nCO_2 \rightarrow 2nCO + \left(\frac{m}{2}\right) H_2 \tag{5}$$

$$\text{Steam reforming}: \ C_nH_m + nH_2O \rightarrow \left(n + \frac{m}{2}\right) H_2 + nCO \tag{6}$$

$$\text{Water gas shift}: \ CO + H_2O \leftrightarrow H_2 + CO_2 \tag{7}$$

The yield of CO_2 decreased and those of CO and H_2 increased for all biomass at temperatures above 1250°C due to dry (equation 5) and steam reforming (equation 6) and the water-gas shift reactions (equation 7).

In the literature [40–43], the larger fractions of H_2 and CO and a lower fraction of CO_2 along with lower yields of char were related to self-gasification in a drop tube reactor. However, according to calculations (see Table S-1) the self-gasification reaction is slow under the present conditions. The differences observed in the char yields between the WMR and DTF were mainly attributed to changes in heating rate and not self-gasification.

3.4. Alkali transformations of herbaceous biomasses

Char alkali. The weight of each inorganic element retained in alfalfa and wheat straw char from DTF is shown in Figure 6, based on the original sample weight. The main difference between the composition of the two fuels was the ash content, which was higher (7.2 %) in alfalfa straw than in wheat straw (4.1 %). Wheat straw char contained predominantly Si, K and Ca elements, whereas the alfalfa straw char mostly consisted of Ca, K, S, Si, P and Mg. The original alfalfa straw was characterized by a high level of K and Ca, and therefore forming mainly K and Ca rich compounds in the char.

The inorganic composition of original wheat straw showed a large fraction of Si (seven times larger than in alfalfa straw), leading to the formation of silicates during devolatilization. Thermodynamic equilibrium calculations of gas and solid phases, performed with the Factsage software, indicated that under reducing conditions potassium in the alfalfa and wheat straw chars was most likely present as chlorides and silicates. In addition, potassium and calcium could be present as carbides in the alfalfa straw. In the wheat straw char, calcium was obtained as a silicate.

Soot inorganic content. The beechwood and straw soot clusters contained both organic matter and minerals as shown in Figure 7. The mineral compounds in the soot arose from the condensation of inorganic species from the gas phase onto the soot. It appeared that the inorganic elements in alfalfa and wheat straw soot mainly consisted of K, Cl and S. The high levels of K and Cl in the soot matter was probably caused by the KCl release under fast heating in the DTF.

As it can be seen in Figure 7, a high level of sulfur (about 0.8 wt. %) was observed in both soot samples. The Factsage equilibrium calculation showed that sulfur was most likely released as H_2S gas, in agreement with literature results [44, 45]. Hydrogen sulfide could possibly react with soot active sites or with metals, as shown by Cal et al. [46]:

$$\mathrm{C} + \mathrm{H_2S} \rightarrow \mathrm{C\text{-}S} + \mathrm{H_2} \tag{8}$$

$$\mathrm{C\text{-}M} + \mathrm{H_2S} \rightarrow \mathrm{C\text{-}M\text{-}S} + \mathrm{H_2} \tag{9}$$

3.5. Solid residue characterization

3.5.1. Particle size and shape analysis of char

The particle size and shape of the original biomass and its char were analyzed by CAMSIZER XT instrument. Prior to the 2D dynamic imaging analysis, the original fuel was sieved to a particle size fraction of 0.2-0.4 mm. As shown in Figures 8 and 9, the results of the particle characterization study indicate nearly 50 % decrease of the characteristic length of pinewood, beechwood and wheat straw during pyrolysis in comparison to the original fuel, while further changes in particle size between 1000 and 1400°C are almost negligible. The particle size of alfalfa straw char remained similar to the original fuel at heat treatment temperatures of 1000-1400°C. This may be attributed to formation of calcium carbonates and silicates (as shown by the Factsage simulation), which form a very stable inorganic matter shell, hindering particle shrinkage.

The particle shape of biomass was characterized using the sphericity (SPHT) and width/length ratio (b/l) parameters. The pinewood char particles showed a near-spherical shape (SPHT = 0.8-0.9; b/l = 0.7-0.8). The beechwood and herbaceous chars obtained cylindrical or rectangular shapes (SPHT = 0.5-0.8; b/l ratios = 0.4-0.7). The results of particles > 0.4 mm in terms of shape description were considered as non-representative due to the low presence of particles in this fraction. It seems that at high heating rates in the DTF (about 10^4°C/s), a biomass particle transforms to one particular shape that stays unchanged with increasing temperature above 1000°C.

3.5.2. Char and soot structure

Char morphology. Figure 10 shows SEM images of wood and herbaceous char, pyrolyzed at 1000 and 1400°C in the drop tube reactor. The wood and herbaceous char particles have undergone softening and melting. At higher temperatures, the char plasticization is attributed to the formation of liquid metaplast due to the depolymerization with subsequent repolymerization and cross-linking, leading to char formation [47]. The differences in cross-linking propensity influence the fluidity of char significantly. The formation of metaplast depends on the complex interaction of all plant cell compounds (holocelluloses, lignin and extractives). Heating rates affect the melting and swelling behavior of biomass, since the relative rates of competing processes for tar formation (bond-breaking, cross-linking, internal mass transport) change with the temperature. The heating rates determine the temperature at which reaction occurs [48], leading at high heating rates to a significant bridge-breaking in biomass before it starts to cross-link and therefore becomes fluid. On one hand, the inorganic matter could conceivably influence the char morphology since potassium and calcium may act as active catalysts, affecting the metaplast formation. On the other hand, the inorganic matter probably does not have sufficient time to affect cross-linking due to the fast bonds breaking at very high heating rates.

The SEM images showed that the pinewood particles lost all features of the parental structure, becoming spherical and porous with large inner cavities, formed from the simultaneous release of a large volatiles fraction. The pinewood particles have undergone stronger melting during fast pyrolysis by forming smooth and near-spherical structures. It is believed that under fast

heating the formation of metaplast is mostly affected by the bond-breaking and cross-linking of organic components present in lignin that is less volatile than holocelluloses. Surprisingly, beechwood char particles were only slightly molten on the outer surface and kept the shape and size characteristics of the parental fuel, contrary to the results of Dall'Ora et al [9].

This observation is most likely caused by the presence of beechwood at a stage of being converted from the water-conducting sapwood to the heartwood, and to formation of tyloses, which are filled with a large quantity of phenolic compounds, lignin, and aromatic substances [49, 50]. The formed phenolic compounds polymerize in insoluble forms, for example in a non-lignin related bio-polymer suberin that makes the wood particle more stable at high heat treatment temperatures [51, 52].

Alfalfa straw and wheat straw have underwent plasticization, but less melting than the pinewood, indicating an effect of ash on the char morphology. The high levels of K and Ca in the herbaceous biomasses could cause less severe plasticization, by catalyzing the conversion of bridges into char links, and therefore increasing polymerization / cross-linking and reducing char fluidity. The alfalfa and wheat straw char obtained two types of a particle shape (elongated cylindrical and near-spherical). The transformation of herbaceous char shapes was probably affected by the presence of potassium and calcium silicates, remaining in the char. The high Ca content in the alfalfa straw could provide additional stability to the char, preserving the particle size of the original fuel.

In the present study, the effect of extractives on the char structural transformations was studied by removing resin, fatty acids, waxes, and phy-

tosterols from the pinewood and beechwood by acetone extraction. Figure 10 shows the char structures of pinewood and beechwood. The pinewood char after the extraction exhibited stronger swelling and enhanced sticking of smaller particles to the surface of larger particles at 1000°C. The beechwood char without extractives showed slightly stronger melting than the non-treated beechwood char. The extractives could affect the char fluidity. The nearly similar levels of K and Ca in the char of non-treated and extracted wood showed that the extraction process did not have an effect on biomass ash content.

Soot morphology. In the fast DTF pyrolysis, the solid sub-micron particles were collected on a filter. The particulate matter at 1250-1400°C was characterized by TEM and SEM microscopy. The collected nano-sized particles were spherical and attached to each other forming long chain-like structures. Due to the near-spherical shape and particle size < 100 nm, the particulate matter on the filter was identified as soot, mixed with inorganic matter as shown in Figure 11.

Interestingly, also larger sub-micron particles of a size > 100 nm were observed in the particulate matter. The wheat straw fast pyrolysis generated larger sub-micron particles of size 100-300 nm, agglomerated with smaller units of size 5-20 nm, while during the wood pyrolysis the particle size was between 20 and 150 nm. The formation of particles of size between 60 nm and 300 nm at high temperatures during fast pyrolysis has not been extensively discussed in the literature before. However, the differences in a carbon nanostructure and graphitization degree may affect soot reactivity as mentioned previously [43, 53].

4. Conclusion

Char yields from the DTF were lower than those obtained in a wire mesh reactor. This was attributed to the higher heating rates in the DTF, while self-gasification by reaction with CO_2 and H_2O was of minor importance. The straw samples showed a significant char yield decrease in the DTF when the temperature was increased from 1000 to 1400°C, whereas the char yields of pinewood ($\approx$ 3.5 %, daf) and beechwood ($\approx$ 7 %, daf) were almost constant at a very low level. It was observed that low fuel alkali content, high temperatures, and fast heating rates lead to low biomass char yields. The results indicated that the influence of alkali on the char yield is more pronounced at low and intermediate heating rates than at fast heating rates in the DTF.

The measured soot yield of wood was 3-7 % higher compared to herbaceous biomass above 1250°C. Leaching of the wheat straw resulted in a reduction of the soot fraction, indicating that suppression of soot by a high potassium content only plays a minor role. However, the higher concentration of lignin and resin acids in the wood could lead to a larger formation of PAH precursors and thus higher soot yields. The lower soot yields in pyrolysis of leached wheat straw compared to alfalfa straw and non-treated wheat straw were related to the removal of organic compounds, and therefore decreased formation of PAH precursors. Significant levels of K, Cl and S elements were found in the straw soot. The particle size of herbaceous soot varied from 5 nm to 300 nm, whereas the wood formed particles from 20 nm to 150 nm.

The pyrolysis process caused the characteristic length of both wood sam-

ples and wheat straw particles to decrease by a factor of two as shown by 2D dynamic imaging analysis, while the pinewood char obtained the most spherical shape. The beechwood and herbaceous char particles retained a cylindrical shape. Scanning electron microscopy on the chars indicated structural transformations of all biomass under fast heating. The chars underwent strong deformation with clear signs of melting and development of macropores at all applied temperatures. The ability of char to melt under the fast heating followed the order pinewood > wheat straw, alfalfa straw > beechwood, and was related to the formation of a metaplast with a stronger contribution of lignin due to its lower volatility and remaining high-temperature stable extractives (suburin, tannin) in the beechwood char. In addition, a significant catalytic effect of K and Ca on the fuel structural changes was observed due to a stronger cross-linking of herbaceous chars, leading to less fluidity. The increased melting of pinewood and beechwood could indicate some influence of extractives on the char morphology.

Acknowledgements

The authors from DTU would like to acknowledge the financial support that they received for this project from Danish Strategic Research Council, DONG Energy, and Vattenfall. We also thank DTU CEN, Gert Beckmann (Retsch Company) and Kawnish Kirtania (LTU) for assisting with TEM/SEM microscopy and CAMSIZER XT measurements and micro GC measurements.

References

[1] Zanzi R, Sjöström K, Björnbom E, Rapid high-temperature pyrolysis in a free-fall reactor, Fuel 75 (1996) 545–50.

[2] Zanzi R, Sjöström K, Björnbom E, Rapid pyrolysis of agricultural residues at high temperature, Biomass Bioenergy 23 (2002) 357–66.

[3] Lu H, Experimental and Modeling Investigations of Biomass Particle Combustion. PhD thesis, Brigham Young University (2006).

[4] Lu K, Ip E, Scott J, Foster P, Vickers M, Baxter LL, Effects of particle shape and size on devolatilization of biomass particle, Fuel 89 (2010) 1156–68.

[5] Sharma RK, Wooten JB, Baliga VL, Martoglio-Smith PA, Hajaligol MR, Characterization of Char from the Pyrolysis of Tobacco, J Agric Food Chem 50 (2002) 771–83.

[6] Baliga V, Sharma R, Miser D, McGrath T, Hajaligol M, Physical characterization of pyrolyzed tobacco and tobacco components, J Anal Appl Pyrolysis 66 (2003) 191–215.

[7] Sharma RK, Wooten JB, Baliga VL, Lin X, Chan G, Hajaligol MR, Characterization of chars from pyrolysis of lignin, Combust Sci Technol 83 (2004) 1469–82.

[8] Cetin E, Moghtaderi B, Gupta R, Wall TF, Influence of pyrolysis conditions on the structure and gasification reactivity of biomass chars, Fuel 83 (2004) 2139–50.

[9] Dall'Ora M, Jensen PA, Jensen AD, Suspension combustion of wood: Influence of pyrolysis conditions on char yield, morphology, and reactivity, Energy Fuels 22 (2008) 2955–62.

[10] Biagini E, Simone M, Tognotti L, Characterization of high heating rate chars of biomass fuels, Proc Combust Inst 32 (2009) 2043–50.

[11] Umeki K, Kirtania K, Chen L, Bhattacharya S, Fuel Particle Conversion of Pulverized Biomass during Pyrolysis in an Entrained Flow Reactor, Ind Eng Chem Res 51 (2012) 13973–79.

[12] Sharma RK, Wooten JB, Baliga VL, Hajaligol MR, Characterization of chars from biomass-derived materials: pectin chars, Fuel 80 (2001) 1825–36.

[13] Davidsson KO, Pettersson JBC, Birch wood particle shrinkage during rapid pyrolysis, Fuel 81 (2002) 263–70.

[14] Svenson J, Pettersson JBC, Davidsson KO, Fast pyrolysis of the main components of birchwood, Combust Sci Technol 176 (2004) 977–90.

[15] Jones JM, Darwell LI, Bridgeman TG, Pourkashanian M, Williams A, An investigation of ther thermal and catalytic behaviour of potassium in biomass combustion, Proc Combust Inst 31 (2007) 1955–63.

[16] Solomon PR, Best PE, Yu ZZ, Charpenay S, An Empirical Model for Coal Fluidity Based on a Macromolecular Network Pyrolysis Model, Energy Fuels 6 (1992) 143–54.

[17] Serio MA, Charpenay S, Bassilakis R, Solomon PR, Measurement and modeling of lignin pyrolysis, Biomass Bioenergy 7 (1994) 107–24.

[18] Marsh H, Walker PL, The effects of impregnation of coal by alkali salts upon carbonization properties, Fuel Process Technol 6 (1979) 61–75.

[19] Wornat MJ, Hurt RH, Yang NYC, Headley TJ, Structural and compositional transformations of biomass chars during combustion, Combust Flame 100(1-2) (1995) 133–45.

[20] Mermoud F, Salvador S, Van de Steene L, Glofier F, Influence of the pyrolysis heating rate on the stead gasification rate of large wood char particles, Fuel 85 (2006) 1473–82.

[21] Trubetskaya A, Jensen PA, Jensen JD, Steibel M, Spliethoff H, Glarborg P, Influence of fast pyrolysis conditions on yield and structural transformation of biomass chars, Fuel Process Tech 140 (2015) 205–14.

[22] Sluiter A, Hames B, Ruiz R, Scarlata C, Sluiter J, Templeton D et al., Determination of Structural Carbohydrates and Lignin in Biomass. Golden (CO): National Renewable Energy Laboratory; 2011 July Report No. NREL/TP-510-42618. Contract No.: DE-AC36-08-GO28308.

[23] Willför S, Hemming J, Leppänen AS, Analysis of extractives in different pulps - Method development, evaluation, and recommendations. Finland: Åbo Akademi University, Laboratory of Wood and Paper Chemistry; 2004-2009 Report No. B1 of the EU COST E41 action "Analytical tools with applications for wood and pulping chemistry".

[24] Hames B, Ruiz R, Scarlata C, Sluiter J, Sluiter A, Preparation of Samples for Compositional Analysis. Golden (CO): National Renewable Energy Laboratory; 2011 June Report No. NREL/TP-510-42620. Contract No.: DE-AC36-99-GO10337.

[25] Thammasouk K, Tandjo D, Penner MH, Influence of Extractives on the Analysis of Herbaceous Biomass, J Agric Food Chem 45 (1997) 437–43.

[26] Göktepe B, Umeki K, Gebart R, Does distance among biomass particles affect soot formation in entrained flow gasification process?, Fuel Process Technol (2015) In Press.

[27] Tremel A, Spliethoff H, Gasification kinetics during entrained flow gasification - Part I; Devolatilisation and char deactivation, Fuel 103 (2013) 663–71.

[28] Tremel A, Reaction Kinetics of Solid Fuels during Entrained Flow Gasification. PhD thesis, TU mü nchen (2012).

[29] Stiess M, Mechanische Verfahrenstechnik 1 (in German), Springer, 1992.

[30] Merkus HG, Particle Size Measurements, Springer, 2009.

[31] Jensen A, Dam-Johansen K, Wojtowicz MA, Serio MA, TG-FTIR Study of the Influence of Potassium Chloride on Wheat Pyrolysis, Energy Fuels 12 (1998) 929–38.

[32] Warnatz J, Maas U, Dibble RW, Combustion, Springer, 1996.

572 [33] Williams A, Jones JM, Ma L, Pourkashanian M, Pollutants from the
573 combustion of solid biomass fuels, Prog Energy Combust Sci 38 (2012)
574 113–37.

575 [34] Evans RJ, Milne TA, Molecular characterization of the pyrolysis of
576 biomass, Energy Fuels 1 (1987) 123–37.

577 [35] Dufour A, Weng J, Jia L, Tang X, Sirjean B, Fournet R, Revealing
578 the chemistry of biomass pyrolysis be means of tunable synchrotron
579 photoionisation-mass spectrometry, RSC Advances 3 (2013) 4786–92.

580 [36] Daily JW, Jarvis MW, Gaston KR, James FW, Nimlos MR, Donohoe
581 BS et al., Elucidation of Biomass Pyrolysis Products Using a Laminar
582 Entrained Flow Reactor and Char Particle Imaging, Energy Fuels 25
583 (2011) 324–36.

584 [37] Ross AB, Junyapoon S, Jones JM, Williams A, Bartle KD, A study
585 of different soots using pyrolysis-GC-MS and comparison with solvent
586 extractable material, J Anal Appl Pyrolysis 74 (2005) 494–501.

587 [38] Rogge WF, Mazurek MA, Hildemann LM, Cass GR, Simoneit BRT,
588 Quantification of urban organic aerosols at a molecular level: identifi-
589 cation, abudance and seasonal variation, Atmos Environ 27(A) (1993)
590 1309–30.

591 [39] Schauer JJ, Kleeman MJ, Cass GR, Simoneit BRT, Measurement of
592 Emissions from Air Pollution Sources. 2. C_1-C_{29} Organic Compounds
593 from Fireplace Combustion of Wood, Environ Sci Technol 35 (2001)
594 1716–28.

[40] Menendez JA, Dominguez A, Fernandez Y, Pis JJ, Evidence of Self-Gasification during the Microwave-Induced Pyrolysis of Coffee Hulls, Energy Fuels 21 (2007) 373–8.

[41] Huang YF, Kuan WH, Chiueh PT, Lo SL, Pyrolysis of biomass by thermal analysis-mass spectrometry (TA-MS), Bioresour Technol 102 (2011) 3527–34.

[42] Sanchez-Silva L, Lopez-Gonzalez D, Villasanor J, Sanchez P, Valverde JL, Thermogravimetric-mass spectrometric analysis of lignoccelulosic and marine biomass pyrolysis, Bioresour Technol 109 (2012) 163–72.

[43] Qin K, Lin W, Jensen PA, Jensen AD, High-temperature entrained flow gasification of biomass, Fuel 93 (2012) 589–600.

[44] Puri BR, Surface complexes on carbons, Chem Phy Carbon 6 (1970) 191–282.

[45] Puri BR, Hazra RS, Carbon-sulfur surface complexes on charcoal, Carbon 9 (1971) 123–34.

[46] Cal MP, Strickler BW, Lizzio AA, Gangwal SK, High temperature hydrogen sulfide adsorption on activated carbon - II. Effects of gas tempearture, gas pressure and sirbent regeneration, Carbon 38 (2000) 1767–74.

[47] Solomon PR, Serio MA, Suuberg EM, Coal pyrolysis: experiments, kinetic rates and mechanisms, Prog Energy Combust Sci 18 (1992) 133–220.

[48] Solomon PR, Hamblen DG, Carangelo RM, Serio MA, Deshpande GV, General Model of Coal Devolatilization, Biomass Bioenergy 2 (1988) 405–22.

[49] Mauseth JD, Botany: an introduction to plant biology, Jones and Barlett Publishers, 2003.

[50] Myburg AA, Sederoff RR, Xylem Structure and Function, Encyclop Life Sci (2001) 1–9.

[51] Pearce RB, Holloway PJ, Suberin in the sapwood of oak (Quercus robur L.): its composition from a compartmentalization barrier and its occurrence in tyloses in undecayed wood, Physiol Plant Path 24 (1984) 71–81.

[52] Pouzoulet J, Pivovaroff AL, Santiego LS, Rolshausen PE, Can vessel dimension explain tolerance toward fungal vascular wilt diseases in woody plants? Lessons from Dutch elm disease and esca disease in grapevine, Front Plant Sci 5 (2014) 1–11.

[53] Septien S, Valin S, Dupont C, Peyrot M, Salvador S, Effect of particle size and temperature on woody biomass fast pyrolysis at high temperature (1000-1400°C), Fuel 97 (2012) 202–10.

Table 1:

Fuel	Pine-wood	Beech-wood	Wheat straw	Alfalfa straw	Leached wheat straw	Pine-wood*	Beech wood*
Proximate analysis							
Moisture, (wt. % ar)	5.1	4.5	5.5	5.2	4.3	5.1	5.1
Ash (550°C), (wt. % db)	0.3	1.4	4.1	7.4	2	0.3	1.5
Volatiles, (wt. % db)	86.6	79.4	77.5	75.9	84.2	84.9	79.3
HHV, (MJ/kg)	21.6	20.2	18.8	19.7	18.7	20.3	20.3
LHV, (MJ/kg)	20.2	19	17.5	16.9	17.4	19	19
Ultimate analysis, (wt. % db)							
C	53.1	50.7	46.6	42.5	45.7	50.1	50
H	6.5	5.9	6.1	6.7	6.6	6	5.8
O	40	41.9	42.5	43.1	45.4	43.5	42.6
N	0.06	0.13	0.6	0.3	0.3	0.05	0.08
S	<0.01	0.02	0.1	0.03	0.02	0.008	0.019
Cl	0.01	0.02	0.1	0.5	0.01	0.005	0.02
Ash compositional analysis, (mg/kg, db)							
Al	10	10	150	600	100	8.3	15.9
Ca	600	2000	2500	12900	1300	620	2090
Fe	20	10	200	-	350	8	10
K	200	3600	11000	28000	1300	250	3700
Mg	100	600	750	1400	350	120	610
Na	30	100	150	1000	50	60	150
P	6	150	550	1900	80	25	120
Si	50	200	8500	2000	6200	33	200
Ti	2	8	10	30	10	1	4

*after extraction

Table 2:

Biomass	**Cellulose**	**Hemi-cellulose**	**Lignin**		**Extractives**	**Protein**
			acid insoluble	**acid soluble**		
Pinewood	38.3	17.8	29.6	1.8	8.8*	0.6
Beechwood	35	19.2	32	1.5	7.5*	1.9
Wheat straw	35.9	18	19.2	6.5	10.1**	6.3
Leached wheat straw	32.1	23.5	13.8	2	13.3**	1.3
Alfalfa straw	18.8	12	14.7	6.8	39.6**	5.1

* acetone extraction ** ethanol-water extraction (room temperature)

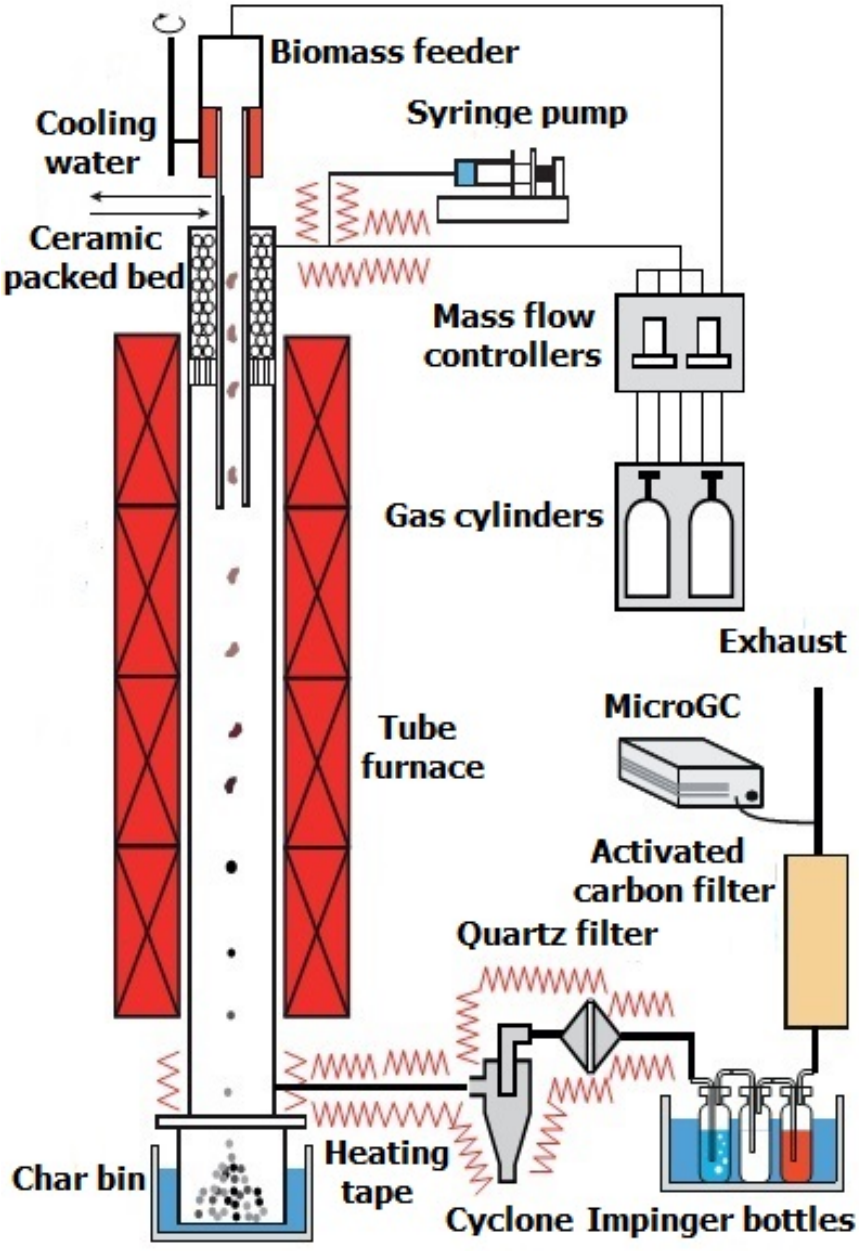
Biomass feeder
Syringe pump
Cooling water
Ceramic packed bed
Mass flow controllers
Gas cylinders
Exhaust
MicroGC
Tube furnace
Activated carbon filter
Quartz filter
Heating tape
Char bin
Cyclone
Impinger bottles

Figure 1

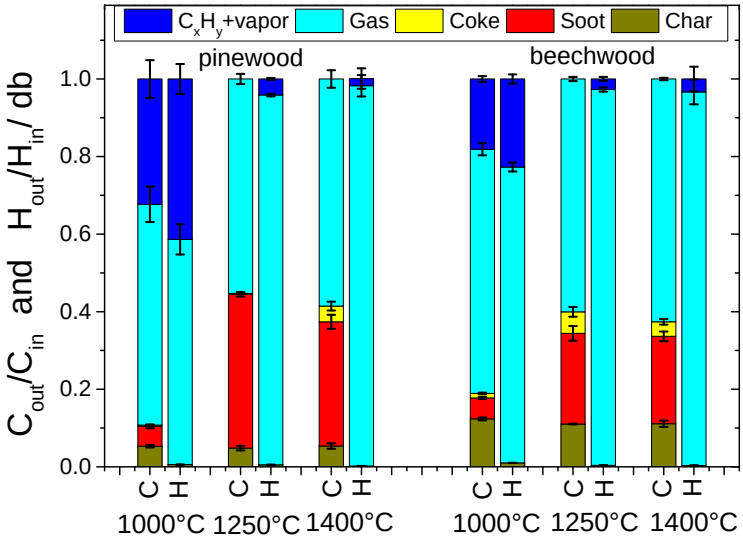

2.1:

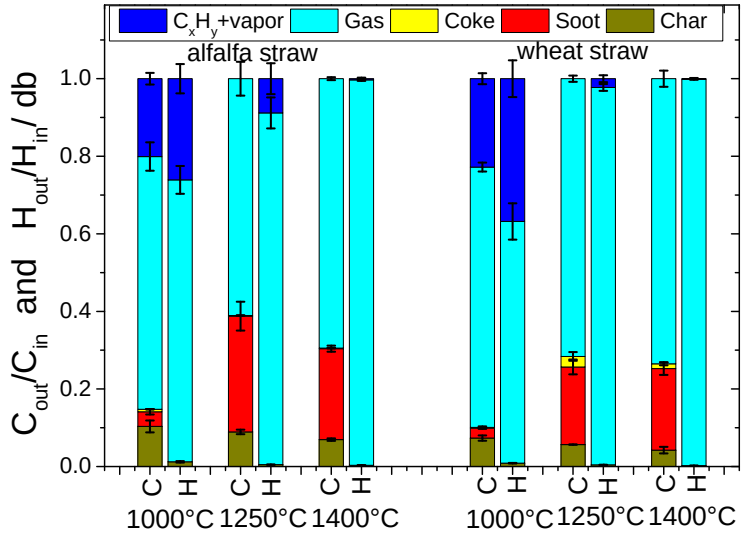

2.2:

Figure 2:

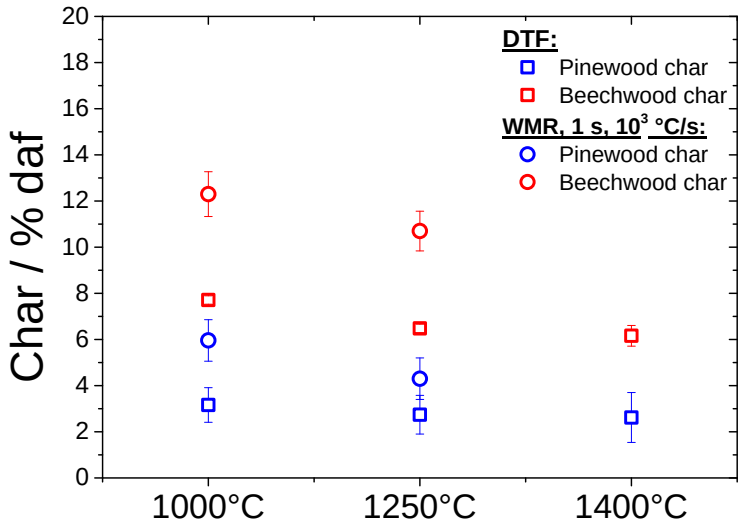

3.1:

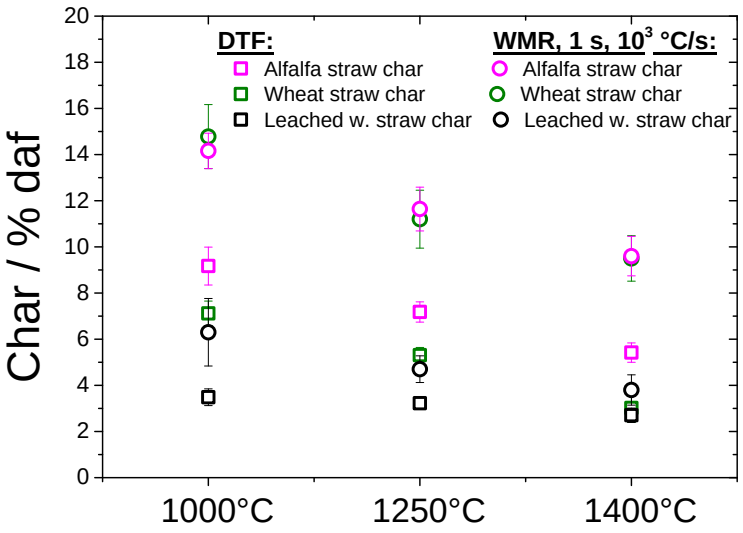

3.2:

Figure 3:

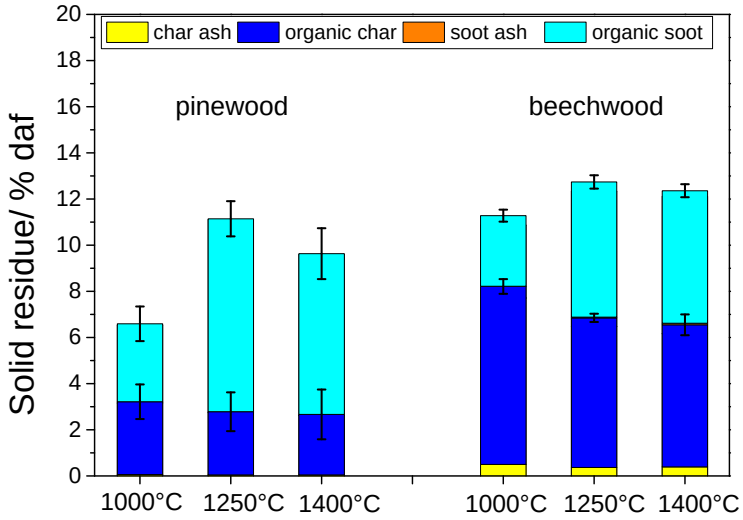

4.1:

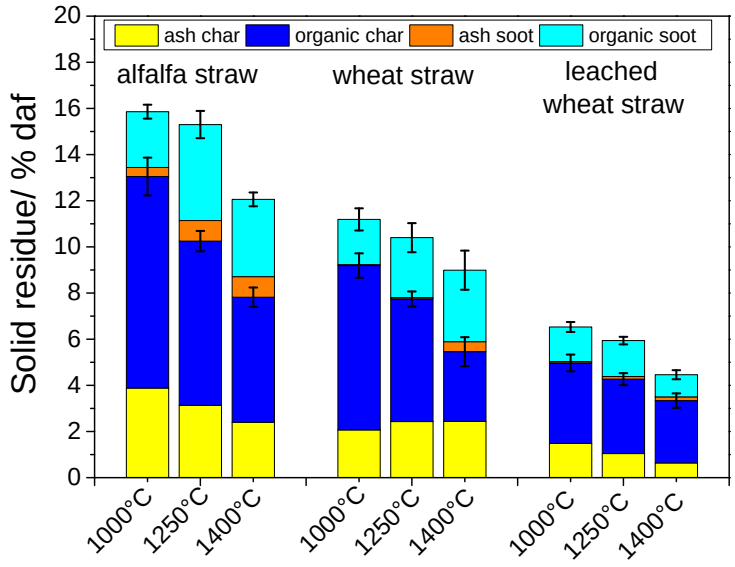

4.2:

Figure 4:

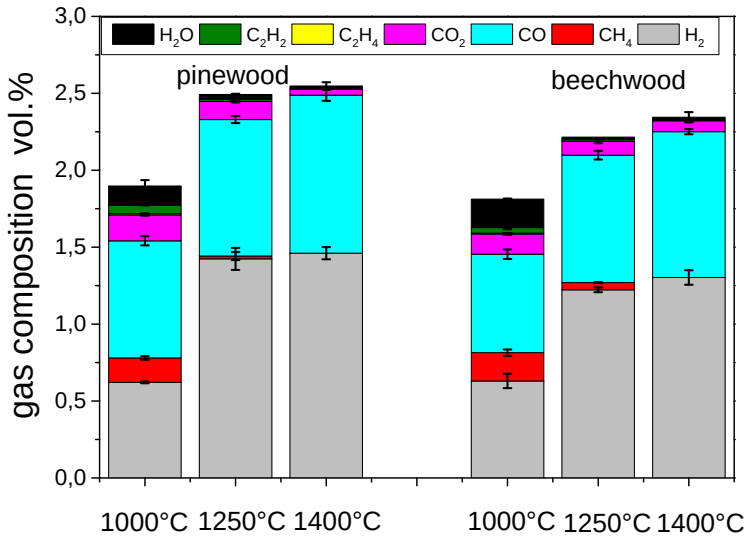

5.1:

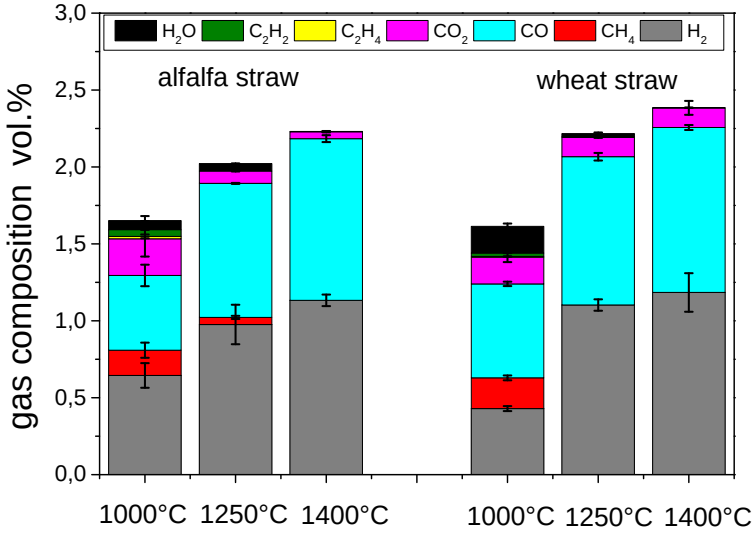

5.2:

Figure 5:

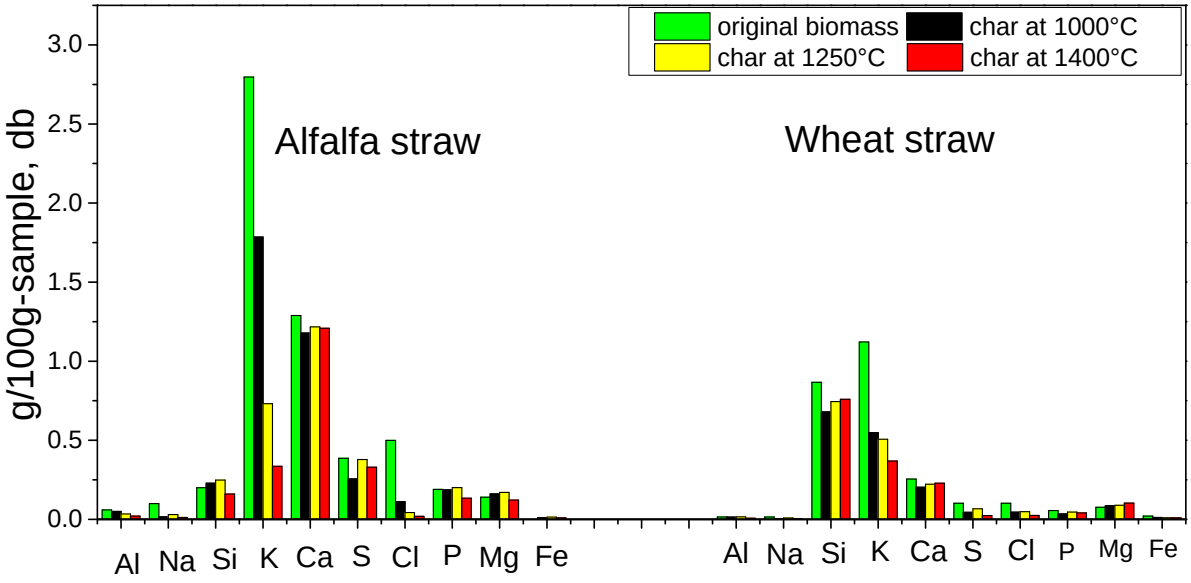
original biomass
char at 1000°C
char at 1250°C
char at 1400°C
Alfalfa straw
Wheat straw
g/100g-sample, db
3.0
2.5
2.0
1.5
1.0
0.5
0.0
Al Na Si K Ca S Cl P Mg Fe
Al Na Si K Ca S Cl P Mg Fe

Figure 6

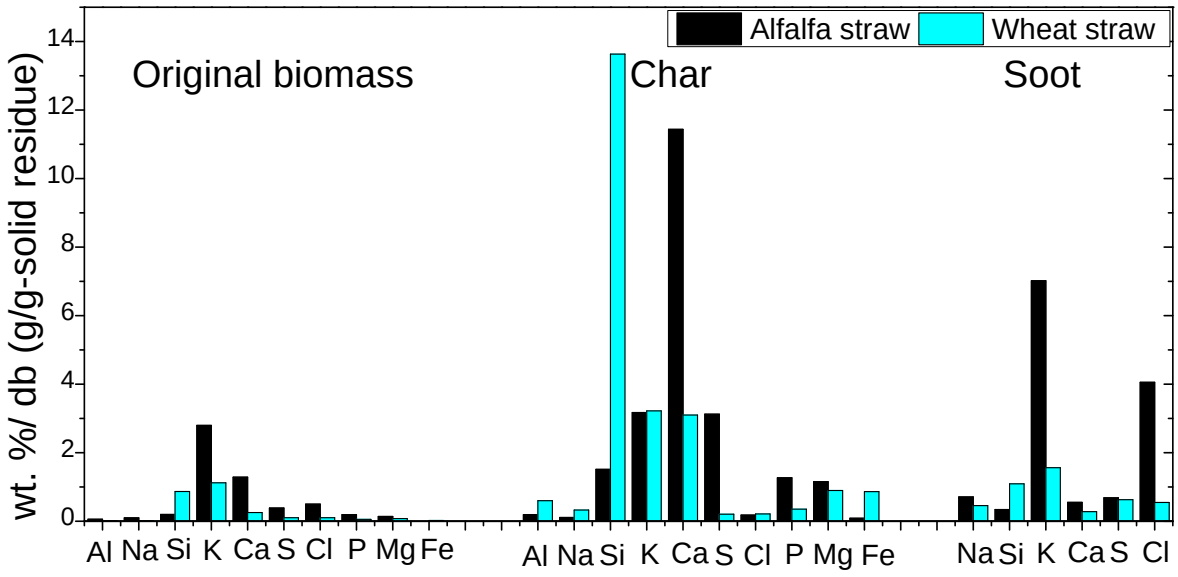
Alfalfa straw
Wheat straw
Original biomass
Char
Soot
wt. %/ db (g/g-solid residue)
0
2
4
6
8
10
12
14
Al Na Si K Ca S Cl P Mg Fe
Al Na Si K Ca S Cl P Mg Fe
Na Si K Ca S Cl

Figure 7

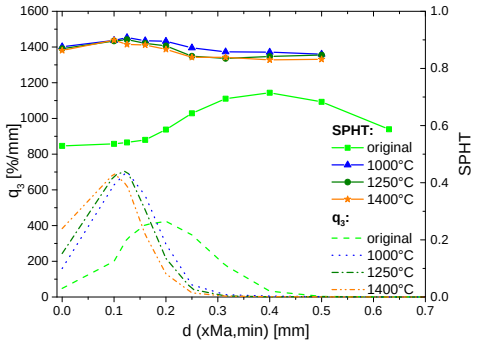

8.1:

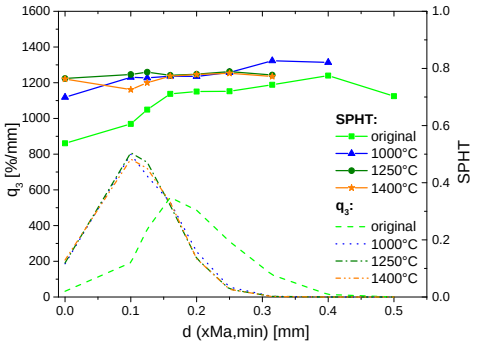

8.2:

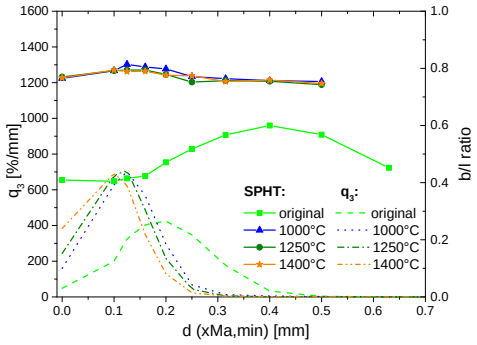

8.3:

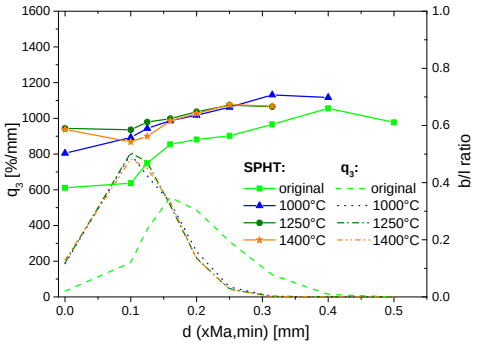

8.4:

Figure 8:

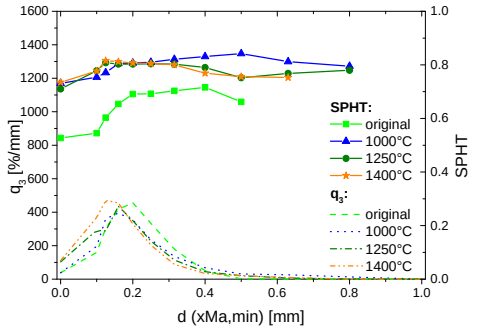

9.1:

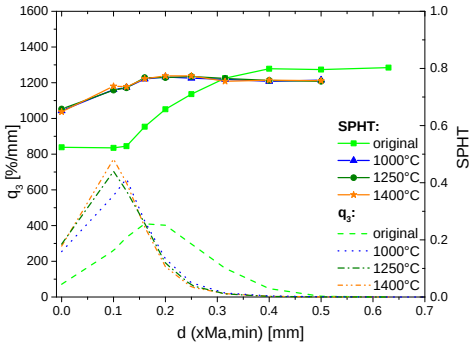

9.2:

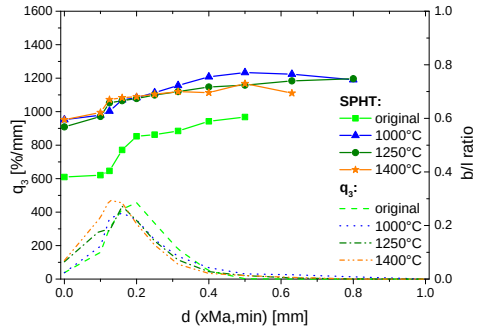

9.3:

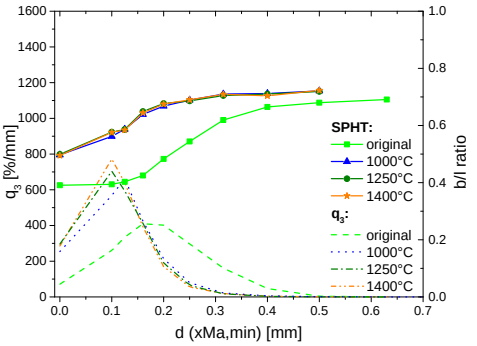

9.4:

Figure 9:

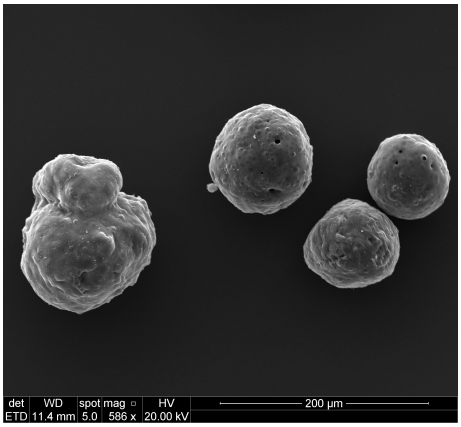

10.1:

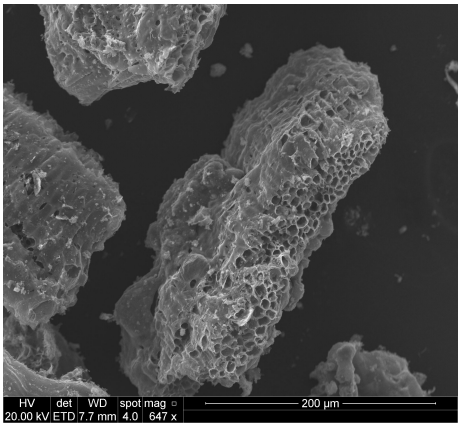

10.2:

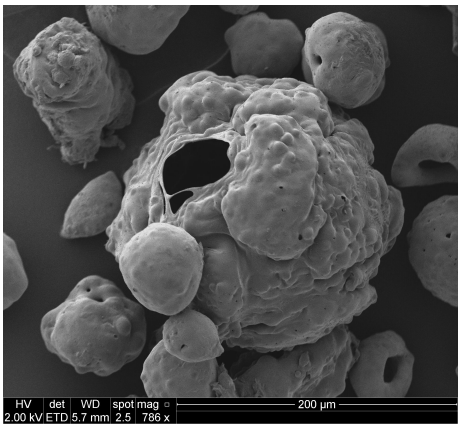

10.3:

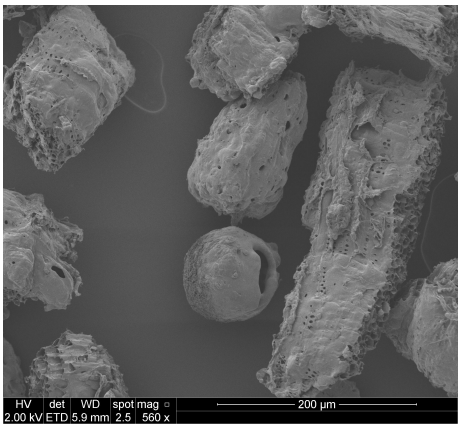

10.4:

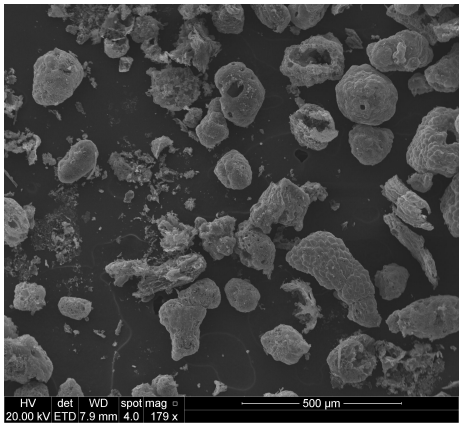

10.5:

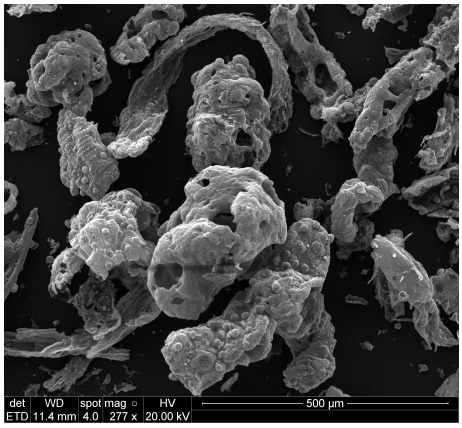

10.6:

Figure 10:

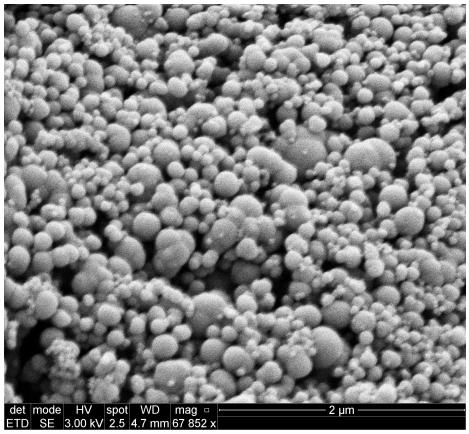

11.1:

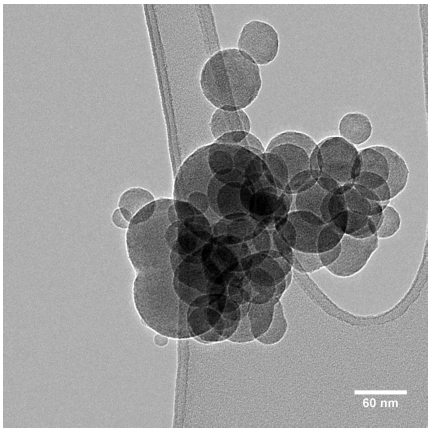

11.2:

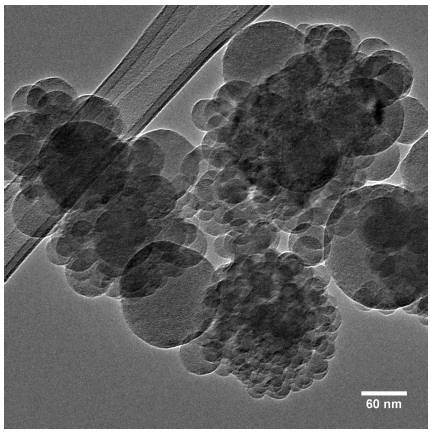

11.3:

Figure 11:

Captions for tables and figures

Table 1: Proximate, ultimate and ash analyses of fuels.

Table 2: Biomass feedstock composition, calculated in percentage based on dry weight (wt. %).

Table 3: Calculation on self-gasification of char ($x_{Ma,min} = 0.1\,mm$) based on parameters derived from TGA measurements in 5 % vol. CO_2 and operational parameters of DTF pyrolysis.

Figure 1. Schematic view of the Drop Tube Reactor at Luleå University of Technology.

Figure 2: Carbon and hydrogen distribution of pinewood, beechwood, wheat straw and alfalfa straw at 1000, 1250 and 1400°C in the DTF.

Figure 2.1: Pinewood and beechwood

Figure 2.2: Alfalfa straw and wheat straw

Figure 3: Char yield comparison of biomass samples, reacted in the WMR and DTF at 1000, 1250 and 1400°C.

Figure 3.1: Pinewood and beechwood

Figure 3.2: Alfalfa straw, wheat straw and leached wheat straw

Figure 4: Soot and char yields (wt. % relative to the original biomass) of pinewood, beechwood, alfalfa straw, wheat straw and leached wheat straw, reacted at 1000-1400°C in the DTF. The total yield of soot and char is separated in ash and organic matters. The error bars characterize the deviations between the total yields of the char and soot.

Figure 4.1: Pinewood and beechwood

Figure 4.2: Alfalfa straw, wheat straw and leached wheat straw

Figure 5: Gas composition of biomass samples from the DTF (vol. % in inert nitrogen), reacted at 1000, 1250 and 1400°C.

Figure 5.1: Pinewood and beechwood

Figure 5.2: Alfalfa straw and wheat straw

Figure 6: Ash elemental retention on the ash basis of original alfalfa and wheat straw and their chars (g/100 g sample), reacted at 1000, 1250 and 1400°C in the DTF.

Figure 7: Ash elemental retention of alfalfa and wheat straw soot and char (g/g of solid residue), reacted at 1400°C.

Figure 8: Particle frequency distribution (q_3), sphericity (SPHT) and width/length ratio (b/l) of original pinewood, beechwood and their chars, reacted at 1000, 1250 and 1400°C.

Figure 8.1: SPHT and q_3 of pinewood

Figure 8.2: SPHT and q_3 of beechwood

Figure 8.3: b/l ratio and q_3 of pinewood

Figure 8.4: b/l ratio and q_3 of beechwood

Figure 9: Particle frequency distribution (q_3), sphericity (SPHT) and width/length ratio (b/l) of original alfalfa straw, wheat straw and their chars, reacted at 1000, 1250 and 1400°C.

Figure 9.1: SPHT and q_3 of alfalfa straw

Figure 9.2: SPHT and q_3 of wheat straw

Figure 9.3: b/l ratio and q_3 of alfalfa straw

Figure 9.4: b/l ratio and q_3 of wheat straw

Figure 10: SEM images of biomass pinewood and beechwood chars, reacted at 1000°C and compared with the pinewood and beechwood after extraction

with acetone, reacted at 1000°C, and alfalfa and wheat straw chars, reacted at 1400°C. SEM images of alfalfa straw and wheat straw were taken under a lower magnification to show at least two particles of a different shape in the same image (elongated and near-spherical).

Figure 10.1: Pinewood

Figure 10.2: Beechwood

Figure 10.3: Pinewood ext.-free

Figure 10.4: Beechwood ext.-free

Figure 10.5: Alfalfa straw

Figure 10.6: Wheat straw

Figure 11: SEM image of pinewood soot, reacted at 1400°C; TEM of beechwood and alfalfa straw soot.

Figure 11.1: Pinewood

Figure 11.2: Beechwood

Figure 11.3: Alfalfa straw